IEEE Open Journal of
Industry Applications

Received 16 March 2023; revised 10 June 2023; accepted 10 August 2023. Date of publication 23 August 2023;
date of current version 7 September 2023. The review of this article was arranged by Associate Editor Brant Cassimere.

Digital Object Identifier 10.1109/OJIA.2023.3307299

Coordinated Decentralized Control of Dynamic Volt-Var Function in Oil and Gas Platform With Wind Power Generation

LORRANA F. DA ROCHA [1,2], DANILO I. BRANDAO [1] (Senior Member, IEEE), KASSIANE DE S. MEDEIROS [1], MATHEUS S. DALL'ASTA [3], AND TELLES B. LAZZARIN [3] (Senior Member, IEEE)

[1]Graduate Program in Electrical Engineering, Universidade Federal de Minas Gerais, Belo Horizonte, MG 31270-901, Brazil
[2]Department of Electric Energy, Norwegian University of Science and Technology, 7034 Trondheim, Norway
[3]Department of Electrical and Electronic Engineering, Federal University of Santa Catarina, Florianopolis, SC 88040-900, Brazil

CORRESPONDING AUTHOR: DANILO I. BRANDAO (e-mail: dibrandao@ufmg.br).

This work was supported by the Research Support Foundation of the State of Minas Gerais – FAPEMIG under Grant PPM-00587-18.

ABSTRACT The integration of offshore wind energy power system is a solution to reduce carbon emissions in the oil and gas sector. However, the intermittent profile of wind power generation can bring challenges of voltage/frequency fluctuations to the electrical grid of the platform. This article proposes a coordinated decentralized control used to mitigate voltage fluctuation in oil and gas platform caused by connection of wind power system through short- and long-umbilical cables. The proposed control is split into optimum loss control embedded in the wind power system control, and modified dynamic volt-var functions applied to active front-end variable frequency drives. The decentralized control is evaluated by means of simulation results considering a real case test bench of a typical Brazilian offshore platform with a wind power system of 10 and 50 MW, and umbilical cable of 12 and 150 km. The results indicate an effective contribution of the dynamic volt-var function in reducing voltage fluctuations for the three implemented wind power system configurations (i.e., 10; 50, and 50 MW/150 km).

INDEX TERMS Coordinated control, offshore wind, O&G platform, voltage fluctuations, volt-var function.

I. INTRODUCTION

Increase oil and gas (O&G) production in offshore platforms is always a motivation to maximize profits and provide more energy, mainly with the discovery of new fields in deep and ultradeep waters [1]. A trivial solution is to insert new diesel or gas turbine generators, however, it would require area and volume in the platform, and increase weight and greenhouse gas (GHG) emissions [2], exceeding established limits by agreements and governmental projects to reduce GHG emissions [3], [4]. Therefore, the integration of renewable energy sources in offshore platforms has recently been discussed [5], [6], [7]. In addition to reducing carbon emissions generated by gas turbines, it would reduce the cost of investments to transmit offshore energy to land.

The offshore platforms are characterized as isolated electrical systems with loads of low efficiency and power quality. As a result, they are more sensitive to disturbances, as they cannot rely on the main grid to maintain voltage and frequency. The high insertion of wind energy conversion system (WECS) through short and long umbilical cables into these weak power systems may cause voltage and frequency oscillations due to the heavy intermittence of wind speed. Methods have been proposed in the literature for stabilizing the wind power output, mainly in large-scale integration. The vast majority of these methods are based on energy storage systems (ESSs) [8], [9], [10], [11], [12], as in addition to smooth the generation, they provide a backup energy for renewable generation. In [8], a short-term ESS is used to smooth out fast wind power changes. Despite the performance effectiveness of the proposed supercapacitor, it is dependent on accurate wind power predictions. In order for the system to be less dependent on prediction errors, larger rated ESS are needed. In [9], different operating constraints are analyzed for the calculation of the capacity and power rating of the ESS.

In [10], the ESS sizing is based on the probabilistic forecast of the wind power and analysis of the wind fluctuation feature. Therefore, the impact of the desired application for the system capacity estimation is noted, showing the need for larger storage for larger wind variations. In order to combine a fast response and low power capacity with a slow response and high power capacity, hybrid storage systems are used to compensate the output power of the wind system. In [11], this hybrid system is composed of a battery and a superconducting flywheel. The authors of [12] proposed a method for virtual inertia capable of reducing the energy storage rating when the inertia response and primary frequency response are deployed. However, inserting ESS in offshore platforms is challenging due to area, volume, and weight limitations and application in harsh environments. Furthermore, it is a challenge to optimally operate the combination of conventional power generation (dispatchable), renewable generation (nondispatchable), and energy storage in an isolated microgrid in a more cost-effective and sustainable manner [13].

Other approaches provide coordinated control of active and reactive power of the wind turbine to smooth voltage variations caused by severe fluctuations in wind speed [14], [15]. In [14], the wind system output power is given considering the relation with the turbine mechanical speed through a lookup table and the current forecasts of wind speed. In [15], voltage fluctuations are compensated by the wind turbine's reactive power control. Furthermore, to keep the voltage within an acceptable range, there is a distribution between the active and reactive powers of the turbine according to wind speed predictions. Although these types of control manage to smooth out voltage fluctuations, they have certain limitations, such as the need for a correct wind speed forecast and active power adjustment in order to achieve the necessary reactive power flow to maintain voltage levels within the permitted operating range. The methods for wind power prediction, for example, have shown efficiency, but there are still drawbacks such as nonlinear dynamics and computational cost [16].

Most of the electrical grids work with a penetration limit of distributed energy resources (DER) due to an intermittent profile of the power flow of renewable energy [17]. Therefore, voltage regulation provided by DER output control itself with a reactive power support might assist to increase the amount of DER into the grid [18]. In the same way, the integration of WECS can help in the grid stability of an O&G platform according to the controls implemented in the wind converters. A dynamic reactive power droop control and a temporary frequency droop control implemented in wind turbines are shown in [6], in order to improve voltage and frequency stability in the platform installations. This implementation takes more advantage of the faster actuation of the wind turbine voltage source converter (VSC) control than the gas turbine governor and automatic voltage regulator (AVR). In addition to droop control, the volt-var function can be applied to converters that interface with the grid, as shown in the literature [19], [20], [21].

Voltage regulators present in traditional grids have a greater response delay than the power fluctuations present in intermittent renewable energies. The analysis in [22] shows that slow-acting grid voltage controllers are the main cause of voltage collapse in a grid with high penetration of these sources. Thus, the inability of well-timed voltage regulation could also cause a violation of regulatory limits such as IEC-61892-1 [23] in offshore grids. Therefore, voltage regulation with a faster response time is required, such as grid interface inverters distributed along the feeder. There has been a tendency to replace direct drive induction motors with variable frequency drive (VFD) in traditional grids in the last decades [24]. On the other hand, VFDs are common in O&G platform grids due to their benefits like: improved energy availability, reduced inrush current during large motor start-up, noncontribution to short-circuit currents, more efficient operation under low load and among many other advantages [25]. Despite the weight and area demanded by VFDs on the platform, the listed advantages justify their use in this type of system. Currently, passive rectifiers are used to interface with the electrical grid. However, there are already commercial solutions with active rectifiers aimed at controlling the reactive power flow exchanged with the platform [26], [27]. One of the disadvantages of inserting VFDs in the platform is the insertion of one more component, which could reduce the total efficiency of the system, however, for medium voltage level, the efficiencies found are up to 99% and 98% without and with the isolation transformer, respectively.

This article proposes a coordinated decentralized control of modified dynamic volt-var function implemented locally in the active front-end VFDs targeting to reduce the voltage fluctuation caused by heavy intermittence of WECS. The volt-var function is widely applied to DER in the main grid, but not yet evaluated on isolated grid of O&G platforms through a decentralized control of VFDs. Moreover, the dynamic volt-var function is modified to provide reactive power support for increasing the power factor at the main supplier. The converter embedded in the WECS does not contribute to the reactive power support and voltage regulation aiming only to maximize the generation of active power and minimize the losses through the umbilical cable. The results are generated based on a real case test bench of a typical Brazilian offshore platform, implemented in MatLab/SimScape and quantitatively evaluated its performance and compared with other conventional solutions considering VFDs without ancillary service.

The rest of this article is organized as follows. Section II shows the system electrical configuration with the parameters used in O&G platform and WECS. The proposed decentralized control is shown in Section III, describing the optimal control of wind generation and the modified dynamic volt-var function applied to the VFDs. Section IV shows simulation results for two power levels of wind generation and two umbilical lengths. Finally, Section V concludes this article.

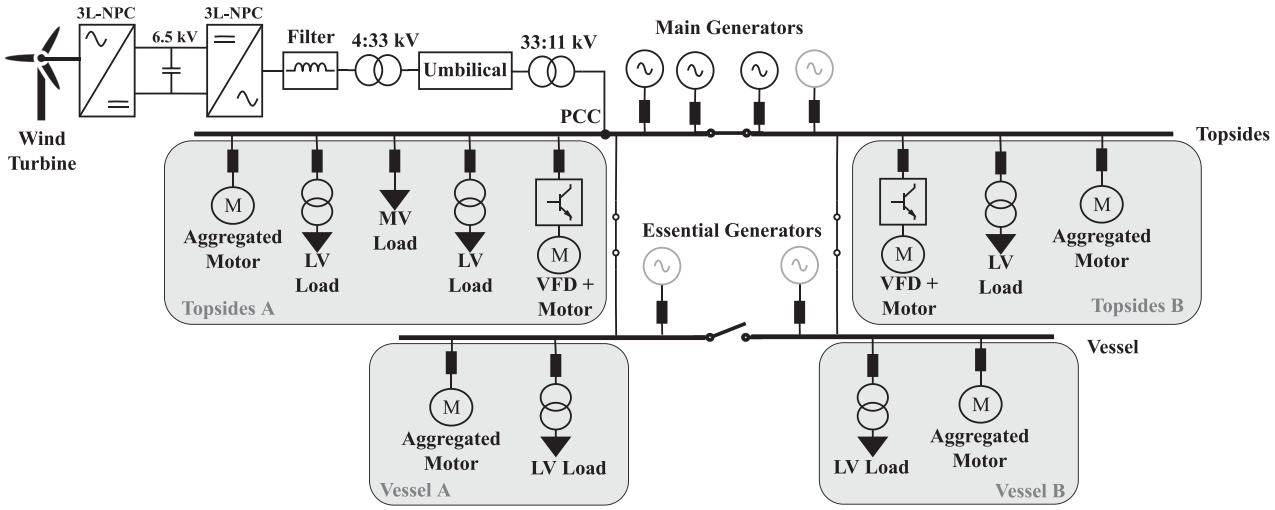

FIGURE 1. Schematic diagram of the electric grid of an offshore oil and gas platform with wind energy conversion system.

II. POWER SYSTEM OF THE OIL AND GAS PLATFORM WITH WIND POWER GENERATION

Fig. 1 describes the electrical power system of a floating production storage and offloading (FPSO) platform, which has two 11 kV, 60 Hz, electrical panels, called Topsides and Vessel. Both panels are split into sides A and B. The system is powered by four 36.25 MVA main synchronous generators (SGs) driven by gas turbines, 28.8 MW each, and two 3.36 MVA essential diesel generators. Three out of four main generators run in parallel to allow any planned maintenance and/or unexpected unit unavailability. The generators are modeled as salient pole synchronous machines with AVR and turbine speed regulators. They are controlled using droop, with the same rated capacity and identically parameterized. However, the secondary regulation of voltage and frequency is not considered herein. Furthermore, the diagram is composed of step-down transformers of 11 kV/720 V connected to the low-voltage loads by the constant power model. Medium-voltage loads comprise induction motors of squirrel-cage rotors. The connection of the induction motors is direct to the grid, except for the two water injection pumps (the highest loads in the platform, 13 MW each), which are connected through the active front-end VFD. Herein, these VFDs are further exploited to reactive power support for voltage regulation and power factor improvement at the terminals of SG [28].

To reduce the system simulation processing time, the model of aggregate motors is used for each side (A and B) of each bus, without loss of generality [29]. As a result, the aggregated motor is represented by a single induction motor with the same dynamic response as the system with individual motors. The only motors outside the aggregate model are the motors connected through the VFDs. The operating mode used contains three main active generators with the following loads located along the four buses: five low-voltage loads and one medium-voltage load with 8.75 MW and 4.89 Mvar of power; 27 induction motors with 78.43 MVA in total and power factors ranging from 0.77 to 0.92. The parameters of the FPSO platform can be found in [30].

The WECS consists of a 10 MW, 10 r/min, three-blade horizontal axis wind turbine directly coupled to a 10.8 MVA, 4 kV, 26.67 Hz, permanent magnet synchronous generator (PMSG). The PMSG operates with variable speed control and tracking algorithm to maximize the generated power from wind speeds ranging from 4 to 11 m/s. Above this threshold, the generator operates at rated speed and the blade pitch control limits its generation at the rated power of 10 MW. A wind turbulence profile is generated with a shaping filter with white noise input [31], in which the filter parameters are adjusted according to the wind profile in the Brazilian southeast coast. This turbulence profile is generated within one second sampling time. Its amplitude is scaled according to the turbulence intensity and then added up to the mean wind speed value.

A three-level neutral point clamped (3L-NPC) rectifier transmits the generated energy to a 6.5-kV dc bus. The dc-bus voltage is controlled by a 3L-NPC inverter with an output *LCL* filter, which also operates with grid-following current control to deliver the energy to the 60 Hz system. A step-up transformer connects the inverter to an umbilical cable for power transmission and a step-down transformer for connection to the platform, as shown in Fig 1. The parameters of the transformer are: $Z_T = 0.005 + j0.0575$ pu and $Y_T = -j0.02$ pu. Two rated power options are used in the WECS, 10 and 50 MW (i.e., aggregated model of five turbines), as well as two distances of umbilical cable, 12 and 150 km.

III. PROPOSED COORDINATED DECENTRALIZED CONTROL

A. OPTIMUM LOSS CONTROL FOR WIND POWER SYSTEM CONNECTED THROUGH UMBILICAL CABLE

The energy transmission from the WECS to the offshore platform is conveyed through an umbilical cable. Such a cable inherits capacitive feature with series impedance. So variations in the injection of active power by the wind turbine cause

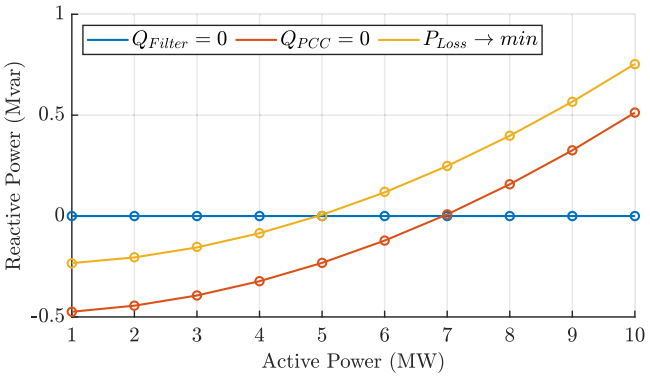

FIGURE 2. Active and reactive power at the output filter of the wind power system for Case 1 (i.e., $\mathbf{Q}_{filter} = \mathbf{0}$), Case 2 (i.e., $\mathbf{Q}_{PCC} = \mathbf{0}$), and Case 3 (i.e., $\mathbf{P}_{loss} \rightarrow$ min). Parameters of the umbilical cable are: 33 kV, 185 mm², 12 km.

reactive power flow variations. The umbilical cable has its length defined according to the distance between the WECS and the offshore platform. In addition, three control strategies are defined in relation to the reactive power control exchanged between the platform and the WECS as

- *Case 1 ($\boldsymbol{Q_{filter} = 0}$):* zero reactive power at the output filter of the wind power system;
- *Case 2 ($\boldsymbol{Q_{PCC} = 0}$):* zero reactive power delivered to the platform;
- *Case 3 ($\boldsymbol{P}_{loss} \rightarrow min$):* minimal losses through the umbilical cable.

For Case 1, $Q_{\text{filter}} = 0$, the reference of the reactive power control (at the output filter) is set to zero regardless of the active power value injected by the WECS, since this variable is directly controlled, as shown in Fig. 2. Therefore, there is a flow of reactive power exchanged between the umbilical and the platform. For Case 2, $Q_{PCC} = 0$, there is no exchange of reactive power between the umbilical and the platform, therefore, the reactive power reference depends on the value of active power injected by the WECS, as shown in Fig. 2. The reactive power reference is established by considering the low-frequency (i.e., 60 Hz) model of umbilical and transformers. The low-frequency characteristics of the umbilical are represented by one-section Π equivalent circuit, and T model for both step-up and step-down transformers. Then, a relation between voltages and currents at the WECS, defined by the subscript 1, and the platform, defined by the subscript 2, is given by

$$\begin{bmatrix} V_1 \\ I_1 \end{bmatrix} = T_1 U T_2 \begin{bmatrix} V_2 \\ I_2 \end{bmatrix} \tag{1}$$

where T_1, U, and T_2 are the matrices of quadripole representations of the step-up transformer, umbilical cable and step-down transformer, which are given as

$$T_k = \begin{bmatrix} 1 + \frac{Z_T Y_T}{2} & Z_T \left(1 + \frac{Z_T Y_T}{4}\right) \\ Y_T & 1 + \frac{Z_T Y_T}{2} \end{bmatrix} \tag{2}$$

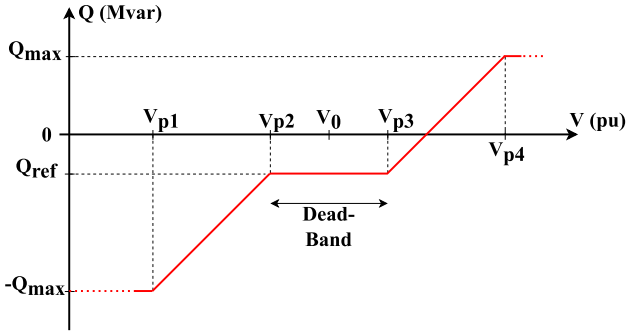

FIGURE 3. Definitions of the volt-var function.

for $k = \{1, 2\}$, and

$$U = \begin{bmatrix} 1 + \frac{Z_U Y_U}{2} & Z_U \\ Y_U \left(1 + \frac{Z_U Y_U}{4}\right) & 1 + \frac{Z_U Y_U}{2} \end{bmatrix}. \tag{3}$$

The values of Z_U and Y_U are computed based on a three-core 33 kV, 185 mm^2 umbilical cable. The analysis considers a voltage magnitude at the platform equal to 1.0 p.u. Then (1) is computed to set the reactive power of WECS ($Q_1 = \text{Im}(V_1 I_1^*)$) as a function of the generated power ($P_1 = \text{Re}(V_1 I_1^*)$) with the condition of zero reactive power delivered to the platform ($Q_2 = \text{Im}(V_2 I_2^*) = 0$). Therefore, it is an open-loop reactive power control based on results from previous steady-state simulations of the system at various operating points.

For Case 3, $P_{\text{loss}} \rightarrow$ min, the reactive power reference also depends on the value of active power injected. However, it establishes the minimum loss ratio through the umbilical cable so that the power delivered by the WECS is maximum, as shown in Fig. 2. In this case, the reactive power injected by the WECS (Q_1) is computed to minimize the transmission losses for each value of generated power:

$$\text{minimize } P_1 - P_2 = f(P_1, Q_1, V_2)$$

$$\text{subject to } \begin{cases} P_1 \leq S_1 \leq S_{\text{max}} \\ V_1 \leq 1.1 \text{ pu} \\ V_2 = 1 \text{ pu} \end{cases} \tag{4}$$

where S_1 is the apparent power delivered by the WECS and S_{max} is the maximum apparent power of the inverter.

B. MODIFIED DYNAMIC VOLT-VAR FUNCTION

Variation in wind speed causes active power variation and thereupon causes voltage fluctuations on the feeders of the platform. To reduce such oscillations, it is proposed to implement the dynamic modified volt-var function in the primary control of the active front-end VFDs connected to the platform. The conventional volt-var curve is modified as shown in Fig. 3. The dead-band defines the voltage value at which the VFDs exchange reactive power with the power system, i.e., V_{p2} and V_{p3}. The points V_{p1}, V_{p4}, and Q_{max} define the inclination of the curves. The point V_0 indicates the midpoint

in relation to the voltage axis as the system does not operate exactly at 1 p.u. The value V_0 is determined by steady-state simulations of the system and changes according to the loading of the platform. Q_{ref} indicates the offset value used to improve the power factor of the system and relieves the main SGs in terms of reactive power since the system loads are mostly inductive.

For cases where the measured voltage is within the limits specified by the dead-band, VFDs process capacitive reactive power according to Q_{ref}. If the voltage on the bus to which they are connected exceeds V_{p3}, then they process reactive power in a coordinated manner to restore acceptable voltage levels. Likewise when the voltage is less than V_{p2}, the VFDs process capacitive reactive power to raise voltage levels. The maximum limit of reactive power injection is described by Q_{max}, computed based on the VFD nameplate rating and active power draw by the motor. Q_{max} is calculated within a control cycle, and it is achieved when the voltage reaches the values V_{p4} and V_{p1}. Note that the volt-var function is an open loop control, and therefore, steady-state deviation may depend on the series impedance of the system.

The reactive power reference Q_{ref} can be computed according to the idle power capacity of the VFD and a certain knowledge of the reactive power demand of the FPSO:

$$Q_{ref} = P_g \times \tan\left[\arccos(fp^*)\right] - Q_{dem} \tag{5}$$

where P_g is the active power demand of the generators, fp^* is the power factor reference to be achieved at the generator output terminals, and Q_{dem} is the reactive power demand of the loads connected to the electrical system of the FPSO.

The volt-var functionality implemented aims to contribute to the reactive power exchange to supply part of the load demand, through the offset value Q_{ref}, and to smooth the voltage fluctuations in the bus, where the VFDs are connected. In a steady state, this extra functionality of active input VFDs can relieve the SG of the FPSO in terms of magnitude of field and armature winding currents, in addition to reducing conductor losses along the platform. During voltage transients, VFDs can support voltage recovery on system buses. The coordinated control architecture is decentralized. Thus, the control algorithm is implemented with only local voltage and current measurements and operates autonomously, i.e., without considering changes in other equipment that participate in the coordinated control. Furthermore, no communication link between the VFDs is required, resulting in standalone converters and high control reliability [32]. However, power factor regulation and power sharing among VFDs are not very accurate since measurements are local and there is no central controller [33].

The modified volt-var function applied to active front-end VFD and optimal loss control embedded in the wind system have no direct connection to each other. While the control of the VFDs aims at reducing voltage variation in the platform's electrical system through local measurements and actions, the control of the wind converters minimizes losses in the umbilical cable that conveys energy from the wind turbine to the FPSO. The active power control of the wind converters acts on the MPPT and does not apply any tool/calculation to reduce the active power oscillation and follows the wind profile applied to the system for the best harvest of energy. It is the reactive power control of wind converters that establishes a ratio of minimum losses across the umbilical cable and delivers maximum power to the FPSO power system.

IV. SIMULATION RESULTS

The electrical power system is developed and simulated in MATLAB/Simulink, using the Simscape library. The configuration of the proposed volt-var curve is: $V_0 = 0.9918$ p.u.; V_{p2},$V_{p3} = V_0 \pm 0.001$; V_{p1},$V_{p4} = V_0 \pm 0.05$. The parameters chosen for the volt-var curve were raised empirically, in which the V_0 is the average value over the voltage oscillation, V_{p2} and V_{p3} are inferior limits to exchange reactive power while V_{p1} and V_{p4} superior limits to saturate reactive power exchanging with the grid. Q_{ref} is changed throughout the simulation to illustrate the impact on the power factor of the main generators.

The results are split into two sections. Section IV-A shows the results for the different reactive control strategies (i.e., $Q_{filter} = 0$, $Q_{PCC} = 0$, and $P_{loss} \rightarrow$ min) of the WECS for a critical wind profile. These three cases are defined to assess the reactive control strategies applied to wind converters and are only related to the control used for the wind converters. On the other hand, the dynamic volt-var function applied in the VFDs is only activated for the case $P_{loss} \rightarrow$ min. The power factor regulation is evaluated by the change of Q_{ref} during the simulation. The rated power of the wind system is P_{wind} = 10 MW and the length of the umbilical cable is L_{umb} = 12 km.

Section IV-B compares the results with and without the dynamic volt-var function for three WECS configurations. Both results use the WECS reactive power control strategy of minimum losses through the umbilical (i.e., $P_{loss} \rightarrow$ min). The average wind speed applied is 9 m/s with a turbulence of 14%. The applied wind turbulence profile is the most critical case of real data obtained from winds of the southeast coast of Brazil from the Mero oil field.

A. WIND POWER SYSTEM CONTROL STRATEGIES AND MODIFIED DYNAMIC VOLT-VAR FUNCTION

Fig. 4 shows the results obtained for the three case studies proposed in Section III-A, i.e., $Q_{filter} = 0$, $Q_{PCC} = 0$, and $P_{loss} \rightarrow$ min, according to the reactive power control strategy of the WECS, and dynamic volt-var function applied to VFDs. At the instant $t = 80$ s, the reactive power reference of the volt-var curve (Q_{ref}) changes from zero to 5.12 Mvar, in order to highlight the open-loop power factor regulation. It also compares the proposed modified volt-var function against the conventional volt-var function in O&G platform.

The wind profile used in the results of Fig. 4 is critical in order to explore the control over the entire power range at the output of the wind system. The active power variation of the wind power system is shown in Fig. 4(a), which has a power

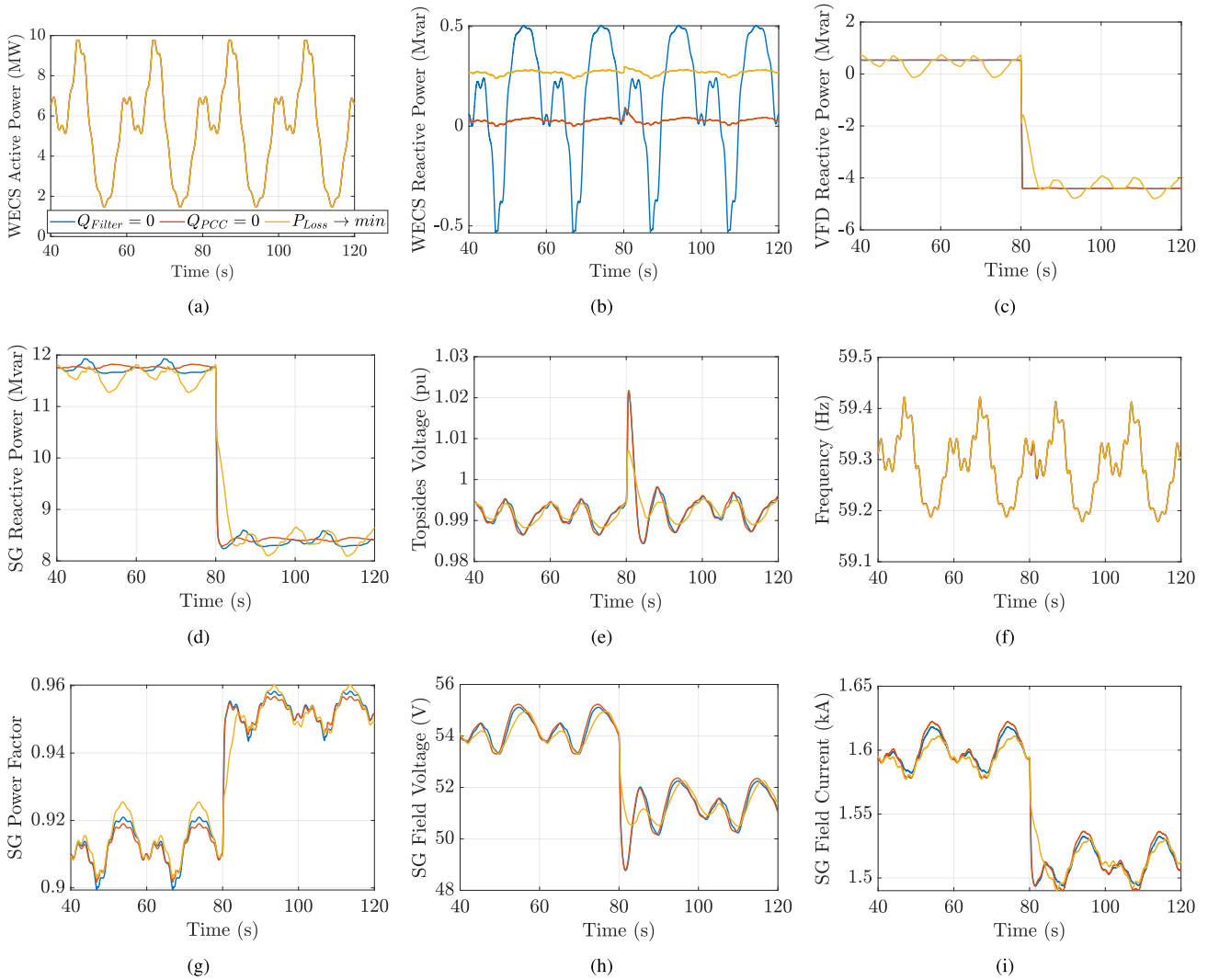

FIGURE 4. Results of cases $Q_{filter} = 0$, $Q_{PCC} = 0$, and $P_{loss} \rightarrow$ min. (a) Active power of the wind system at the coupling point. (b) Reactive power of the wind system at the coupling point. (c) Reactive power of one of the motors with VFD. (d) Reactive power from one of the main generators. (e) Voltage on the Topsides bus. (f) Topsides electrical frequency. (g) Main generator power factor. (h) Main generator field voltage, and (i) Main generator field current.

variation of 8.54 MW in a period of approximately 7 s. The differences in the reactive power control strategies of the wind system for the three cases can be seen in Fig. 4(b). The curves in Fig. 4(b) prove the correct functioning of the implemented control strategies, where the curve of $Q_{\text{filter}} = 0$ (blue) shows a variable flow of reactive power between the platform and the umbilical cable, the curve of $Q_{PCC} = 0$ (red) represents the power flow close to zero of the umbilical with the platform, and the curve of $P_{\text{loss}} \rightarrow$ min (yellow) represents a constant flow of reactive power between the umbilical and the platform.

$Q_{\text{filter}} = 0$ and $Q_{PCC} = 0$ do not have reactive power oscillation in motors with VFD, Fig. 4(c), since the reference of the control is established only by Q_{ref} (i.e., with no dynamic volt-var function). Differently from what happens for $P_{\text{loss}} \rightarrow$ min in which it is noticed the reactive power varies according to the voltage oscillation (with dynamic volt-var function). At the instant $t = 80$ s, Q_{ref} changes from zero to 5.12 Mvar. Therefore, the reactive power of the main SG, Fig. 4(d), decreases at the same instant due to the variation of Q_{ref} as the VFDs increase their reactive power compensation on the platform. Only the curve of one of the SGs is shown in the results and the same goes for curves related to VFDs since they are equal.

It can be noted that the voltage variation, Fig. 4(e), is greater for $Q_{\text{filter}} = 0$ and $Q_{PCC} = 0$ than for $P_{\text{loss}} \rightarrow$ min due to the use of the dynamic volt-var curve. The voltage variation of the Topsides bus, considering the maximum and minimum voltage within the steady state, can be seen in Table 1. Analyzing the results, it is seen a reduction in the voltage fluctuation caused by the integration of the WECS through the application of the dynamic volt-var curve. The active front-end VFD contributed to a reduction of about 34%, in $P_{\text{loss}} \rightarrow$ min, in relation to $Q_{\text{filter}} = 0$ and $Q_{PCC} = 0$. On the other hand, the dynamic volt-var function has no impact on the electrical frequency of the system as shown in Fig. 4(f). It is worth noting that for the correct adjustment of the parameters of the

TABLE 1. Voltage Variation and Power Loss Through the Umbilical for Case Studies in Section IV-A

Cases	ΔV (60 – 80 s)	ΔV (100 – 120 s)	Umbilical
	PF = 0.91	PF = 0.95	P_{loss}
$Q_{filter} = 0$	96.12 V	105.36 V	101.28 kW
$Q_{PCC} = 0$	97.66 V	105.84 V	101.17 kW
$P_{loss} \rightarrow$ min	66.39 V	69.05 V	101.12 kW

TABLE 2. Voltage Variation and Power Loss Through the Umbilical for Case Studies in Section IV-B

Volt-var	10 MW/12 km	50 MW/12 km	50 MW/150 km
Off	ΔV = 60.2 V	ΔV = 256.1 V	ΔV = 482.6 V
On	ΔV = 37.8 V	ΔV = 118.2 V	ΔV = 151.6 V
$\frac{\Delta V_{off} - \Delta V_{on}}{\Delta V_{off}}$	37.2%	53.8%	68.6%
Off	P_{loss} = 0.07 MW	P_{loss} = 0.33 MW	P_{loss} = 3.54 MW
On	P_{loss} = 0.07 MW	P_{loss} = 0.33 MW	P_{loss} = 3.53 MW

volt-var curve, it is necessary to previously know the typical system operation, which is not critical for offshore platforms since loads are well-known for each system operating point. In addition, the reactive power control strategies of the wind system do not have an effective contribution to voltage fluctuation. It is also seen a slight reduction in umbilical cable losses (<1%) using strategy $P_{\text{loss}} \rightarrow$ min compared to strategies $Q_{\text{PCC}} = 0$ and $Q_{\text{filter}} = 0$. The loss shown in Table 1 represents the average value within the range of 40 to 120 s. Such a loss reduction increases with increasing the umbilical length.

At the instant $t = 80$ s, the power factor value increases while the field voltage and current values decrease in the main generators as shown in Fig. 4(g), (h), and (i), respectively. This shows the superiority of the modified volt-var function in relation to the conventional one, which would not improve the power factor. The increase in the power factor by 4% provides an increase in the efficiency of the generators. For the generator model used, when operating with FP = 0.8 the efficiency is 95.9% and for FP = 1 the efficiency is 96.4%. In addition, the reduction of field voltage and current brings a thermal relief of the field winding representing for the machine a lower level of excitation and, consequently, a greater margin for it to supply the reactive power. Therefore, the VFDs exploit more functionalities than only driving the variable speed of motors.

B. PERFORMANCE OF VOLT-VAR FUNCTION IN THREE WIND POWER SYSTEM CONFIGURATIONS

The three wind power system configurations implemented in this section are as follows:

- **Configuration 1:** $P_{\text{wind}} = 10$ MW and $L_{\text{umb}} = 12$ km;
- **Configuration 2:** $P_{\text{wind}} = 50$ MW and $L_{\text{umb}} = 12$ km;
- **Configuration 3:** $P_{\text{wind}} = 50$ MW and $L_{\text{umb}} = 150$ km.

Fig. 5 shows the results obtained for these configurations. The reference power is kept constant and equal to $Q_{\text{ref}} = 5.12$ Mvar. The increase in wind power injected into the system and in the length of the umbilical cable increase the topsides voltage variations, both for the system without and with the dynamic volt-var function. The voltage variations obtained between 40 and 110 s are described in Table 2 according to Fig. 5(a), (d), and (g). Enabling the volt-var function on the VFD controls reduces the voltage variation by 37.2% for configuration 10 MW/12 km, 53.8% for 50 MW/12 km, and 68.6% for 50 MW/150 km.

The increase in wind power raised the average voltage of the platform's Topsides bus. Therefore, the configuration 10 MW/12 km and 50 MW/12 km show a reduction in the efforts of the VFDs in terms of reactive power. Configuration 50 MW/150 km has the highest average voltage and lowest absolute mean value of reactive power of the VFDs. For this configuration, there is the greatest loss in the umbilical cable (150 km), where the average loss during the simulation period is around 3.5 MW.

C. LIMITATIONS AND CHALLENGES OF THE PROPOSED VOLT-VAR FUNCTION

The previous results evaluated the potential gains of the electrical system considering the insertion of the active front-end VFD in the FPSO with the modified volt-var function. Large motors are commonly driven by passive front-end VFDs due to advantages like improved energy availability and reduced inrush current during large motor startups. Consequently, these converters should be replaced by active front-end VFDs. Moreover, it would be necessary to adapt the control scheme to exchange reactive power with the grid and ensure the converter's nameplate rating. Therefore, such an approach is more appealing to new FPSO units which will go into operation, where the active front-end VFD is considered in the design phase. There are already active VFDs available on the market [26], [27]. A selection of converters can be made taking into account market availability, costs, reliability, weight, volume, area, efficiency, and offshore applicability. However, it is out of the scope of this article.

FPSOs have constraints on volume, area, and weight, so adding another physical component might be tough in this hostile environment. To better exploit the converters already present on the platform, the dynamic volt-var function adds new functionality to their control by utilizing the idle power capability of VFDs. Other options, such as thyristor-controlled reactor, static voltage compensator, and static reactive compensator, would therefore require additional equipment and produce equivalent outcomes and, thus, they were not evaluated. In addition, the solution based on ESS could bring different results, but it would require a footprint, is expensive, and needs maintenance.

The limitations related to the definition of the volt-var curve parameters are established due to the prior knowledge of the FPSO load profile. The reactive power reference Q_{ref} needs

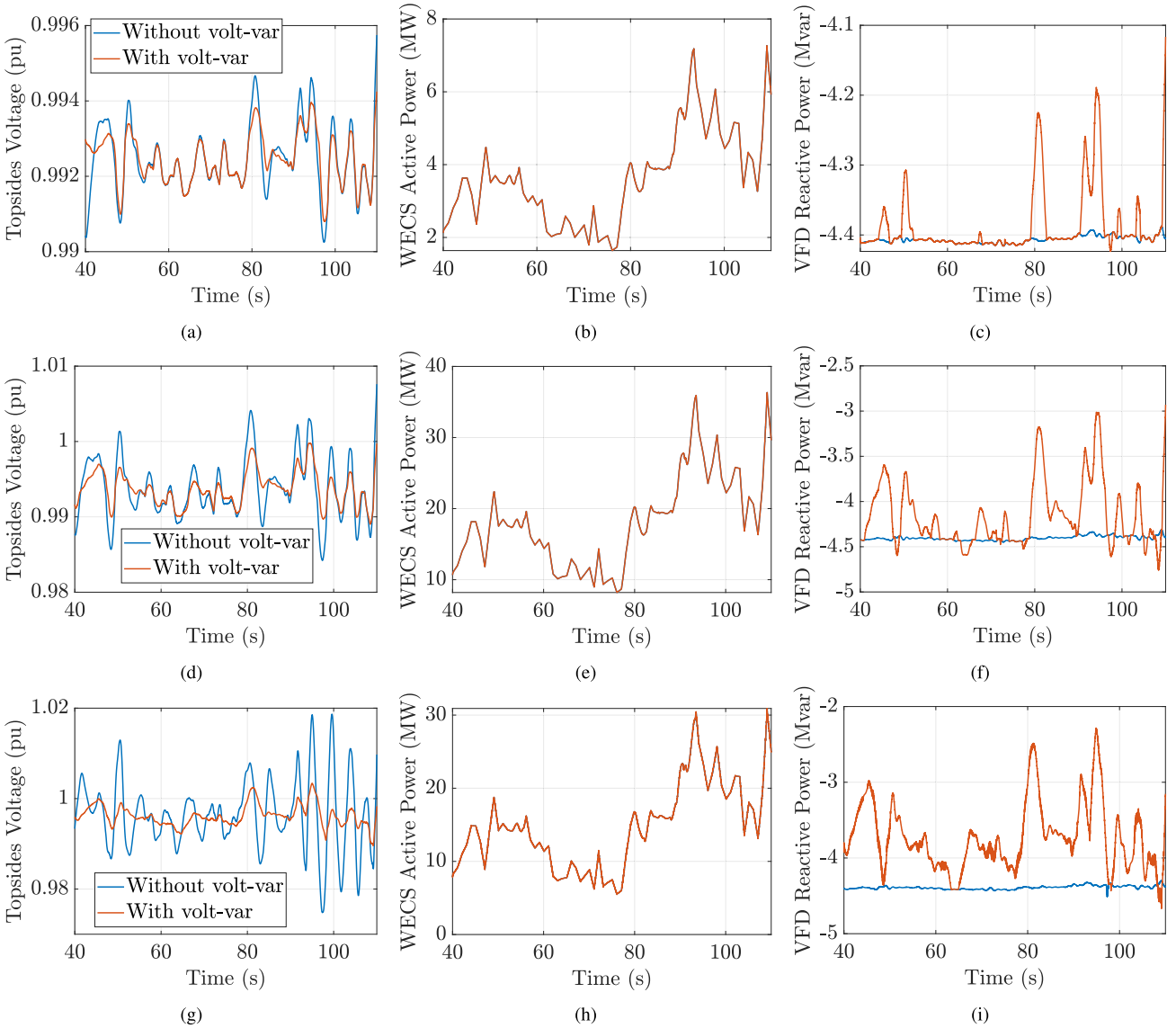

FIGURE 5. Results of 10 MW/12 km: (a) voltage on the Topsides bus, (b) active power of the wind system at the coupling point, and (c) reactive power of one of the motors with VFD. Results of 50 MW/12 km: (d) voltage on the Topsides bus, (e) active power of the wind system at the coupling point, and (f) reactive power of one of the motors with VFD. Results of 50 MW/150 km: (g) voltage on the Topsides bus, (h) active power of the wind system at the coupling point, and (i) reactive power of one of the motors with VFD.

to be calculated for each load profile. The voltage profile of the system also needs to be taken into account to define the midpoint and dead-band of the function. In the results shown, the steady-state voltage is not 1 p.u. because secondary voltage control is not implemented in the system. Therefore, the midpoint of the voltage axis of the volt-var curve is defined by simulating the system in a steady state. However, this would not be a problem for the system in practice, since it would operate at 1 p.u. considering the secondary voltage/frequency control. Although no more rigorous approach has been used for the optimal choice of volt-var curve parameters. Several values were tested in the simulation that represents a real test bench case of a typical Brazilian offshore platform.

The decentralized coordinated control structure is based on agents that operate in an autonomous coordinated manner, without conflicts of interest and seeking to achieve the same objective, but without the need for a communication infrastructure. Despite the autonomous feature and the plug-and-play capability, the decentralized coordinated control does not have the ability to accurately regulate the power flow at a given point in the electrical system, as it only has access to local measurements. As a result, it is not always possible to achieve an optimal system condition, that is, unity power factor at the main generator terminals. However, this does not have a considerable impact on the system since the optimal condition is often not achievable either due to the reactive power injection limitations of the converters that normally

operate with the maximum injection. Furthermore, the open-loop control inaccuracies are not substantial when the system load profile is well known, which is the case with an FPSO unit.

V. CONCLUSION

This article proposed a coordinated decentralized control of the dynamic volt-var function to reduce the voltage fluctuations caused by the insertion of wind energy in an oil and gas platform. The control is applied in two active front-end variable frequency drives. In addition, three strategies for regulating the reactive power of the wind power system are evaluated, in which the minimum losses through the umbilical are preferable.

The voltage fluctuations caused by wind power variation do not exceed the regulatory limits. Nevertheless, the volt-var function achieved a reduction in voltage variation of 68.6% for the wind system configuration of 150 km and 50 MW, the most critical case among the simulated configurations.

Moreover, the coordinated decentralized control implemented through the offset value in the modified volt-var curve regulated in an open loop the power factor. It improved in 4% the power factor at the terminals of the synchronous generator. Thus, a centralized control approach to regulate the power factor in a closed loop, more accurately in tracking the reference, together with the implementation of the dynamic volt-var curve will be investigated in future works. In addition, it is possible to narrow the dead-band or even remove it from the modified dynamic volt-var based on the best configuration of the oil and gas platform.

Although the implemented simulation is sufficient to verify the proposed method, the next step would be a real-time implementation in hardware-in-the-loop. A more thorough detailing of the system and the identification of potential improvements would be feasible by this operation, which would enable the implementation of virtual models that are closer to the real hardware. Furthermore, other figures of merit will be considered in future works, such as system stability, response time, and reliability.

REFERENCES

[1] R. N. Fard and E. Tedeschi, "Integration of distributed energy resources into offshore and subsea grids," *CPSS Trans. Power Electron. Appl.*, vol. 3, no. 1, pp. 36–45, 2018.

[2] Z. Li et al., "Reducing carbon footprint of deep-sea oil and gas field exploitation by optimization for floating production storage and offloading," *Appl. Energy*, vol. 261, 2020, Art. no. 114398.

[3] Oil and gas for the 21st century (strategy document). OG21. Accessed: Jan. 2022. [Online]. Available: https://www.og21.no/en/strategy-and-analyses/the-og21-strategy/

[4] EU Emissions Trading System. EU ETS. Accessed: Jan. 2022. [Online]. Available: https://ec.europa.eu/clima/policies/etsen

[5] W. He et al., "The potential of integrating wind power with offshore oil and gas platforms," *Wind Eng.*, vol. 34, no. 2, pp. 125–137, 2010.

[6] A. R. Årdal, T. Undeland, and K. Sharifabadi, "Voltage and frequency control in offshore wind turbines connected to isolated oil platform power systems," *Energy Procedia*, vol. 24, pp. 229–236, 2012.

[7] S. Sanchez, E. Tedeschi, J. Silva, M. Jafar, and A. Marichalar, "Smart load management of water injection systems in offshore oil and gas platforms integrating wind power," *IET Renewable Power Gener.*, vol. 11, no. 9, pp. 1153–1162, 2017.

[8] C. Abbey and G. Joos, "Supercapacitor energy storage for wind energy applications," *IEEE Trans. Ind. Appl.*, vol. 43, no. 3, pp. 769–776, May/Jun. 2007.

[9] M.-S. Lu, C.-L. Chang, W.-J. Lee, and L. Wang, "Combining the wind power generation system with energy storage equipment," *IEEE Trans. Ind. Appl.*, vol. 45, no. 6, pp. 2109–2115, Nov./Dec. 2009.

[10] J. Shi, W.-J. Lee, and X. Liu, "Generation scheduling optimization of wind-energy storage system based on wind power output fluctuation features," *IEEE Trans. Ind. Appl.*, vol. 54, no. 1, pp. 10–17, Jan./Feb. 2018.

[11] H. Lee, B. Y. Shin, S. Han, S. Jung, B. Park, and G. Jang, "Compensation for the power fluctuation of the large scale wind farm using hybrid energy storage applications," *IEEE Trans. Appl. Supercond.*, vol. 22, no. 3, pp. 5701904–5701904, Jun. 2012.

[12] A. A. Adeyemo and E. Tedeschi, "Sizing of energy storage for virtual inertia emulation and primary frequency control in low-inertia systems," in *Proc. 5th Int. Conf. Power Energy Appl.*, 2022, pp. 480–486.

[13] S. Chapaloglou, D. Varagnolo, F. Marra, and E. Tedeschi, "Data-driven energy management of isolated power systems under rapidly varying operating conditions," *Appl. Energy*, vol. 314, 2022, Art. no. 118906.

[14] C. Luo, H. Banakar, B. Shen, and B.-T. Ooi, "Strategies to smooth wind power fluctuations of wind turbine generator," *IEEE Trans. Energy Convers.*, vol. 22, no. 2, pp. 341–349, Jun. 2007.

[15] J. Ouyang, M. Li, Z. Zhang, and T. Tang, "Multi-timescale active and reactive power-coordinated control of large-scale wind integrated power system for severe wind speed fluctuation," *IEEE Access*, vol. 7, pp. 51201–51210, 2019.

[16] Z. Ma and G. Mei, "A hybrid attention-based deep learning approach for wind power prediction," *Appl. Energy*, vol. 323, 2022, Art. no. 119608, doi: https://doi.org/10.1016/j.apenergy.2022.119608.

[17] J. Barr and R. Majumder, "Integration of distributed generation in the volt/VAR management system for active distribution networks," *IEEE Trans. Smart Grid*, vol. 6, no. 2, pp. 576–586, Mar. 2015.

[18] R. Haider and A. M. Annaswamy, "A hybrid architecture for volt-VAR control in active distribution grids," *Appl. Energy*, vol. 312, 2022, Art. no. 118735.

[19] Q. Li, Y. Zhang, T. Ji, X. Lin, and Z. Cai, "Volt/VAR control for power grids with connections of large-scale wind farms: A review," *IEEE Access*, vol. 6, pp. 26675–26692, 2018.

[20] H. Sun et al., "Review of challenges and research opportunities for voltage control in smart grids," *IEEE Trans. Power Syst.*, vol. 34, no. 4, pp. 2790–2801, Jul. 2019.

[21] H. Peng, S. Huang, Q. Wu, F. Shen, W. Liao, and X. Li, "Decentralized volt/VAR control based on variable gradient projection for PMSG-based wind farm," *IEEE Trans. Sustain. Energy*, vol. 13, no. 3, pp. 1305–1314, Jul. 2022.

[22] S. Maharjan, D. Sampath Kumar, and A. M. Khambadkone, "Enhancing the voltage stability of distribution network during pv ramping conditions with variable speed drive loads," *Appl. Energy*, vol. 264, 2020, Art. no. 114733.

[23] *Mobile and Fixed Offshore Units—Electrical Installations—Part 1: General Requirements and Conditions*, Standard IEC 61892-1:2019, 2019.

[24] P. Waide and C. U. Brunner, "Energy-efficiency policy opportunities for electric motor-driven systems," *IEA*, 2011, Accessed: Jul. 2022. [Online]. Available: https://www.iea.org/reports/energy-efficiency-policy-opportunities-for-electric-motor-driven-systems

[25] P. Pandele, E. Thibaut, and E. Meyer, "All-electrical FPSO scheme with variable-speed drive systems," *IEEE Trans. Ind. Appl.*, vol. 49, no. 3, pp. 1188–1197, May/Jun. 2013.

[26] G. Power Conversion, Medium voltage AC drive: MV7000 press pack. Accessed: Jan. 2022. [Online]. Available: https://www.gepowerconversion.com/product-solutions/medium-voltage-drives/mv7000

[27] WEG, Medium voltage drive - MVW01. Accessed: Jan. 2022. [Online]. Available: https://www.weg.net/catalog/weg/US/en/Drives/Variable-Speed-Drives/Medium-Voltage-Variable-Speed-Drives/C/Global-Wdc-Drv_If-Mv

[28] J. M. S. callegari, L. A. Vitoi, and D. I. Brandao, "VFD-based coordinated multi-stage centralized/decentralized control to support offshore electrical power systems," *IEEE Trans. Smart Grid*, vol. 14, no. 4, pp. 2863–2873, Jul. 2023.

[29] J. Pedra, L. Sainz, and F. Corcoles, "Study of aggregate models for squirrel-cage induction motors," *IEEE Trans. Power Syst.*, vol. 20, no. 3, pp. 1519–1527, Aug. 2005.
[30] H. M. A. Antunes, D. I. Brandao, V. H. M. Biajo, M. H. S. Alves, F. S. Oliveira, and S. M. Silva, "Floating, production, storage, and offloading unit: A case study using variable frequency drives," in *Proc. IEEE Ind. Appl. Soc. Annu. Meeting*, 2022, pp. 1–6.
[31] C. Nichita, D. Luca, B. Dakyo, and E. Ceanga, "Large band simulation of the wind speed for real time wind turbine simulators," *IEEE Trans. Energy Convers.*, vol. 17, no. 4, pp. 523–529, Dec. 2002.
[32] S. Nowak, L. Wang, and M. S. Metcalfe, "Two-level centralized and local voltage control in distribution systems mitigating effects of highly intermittent renewable generation," *Int. J. Elect. Power Energy Syst.*, vol. 119, 2020, Art. no. 105858.
[33] P. Li et al., "Combined decentralized and local voltage control strategy of soft open points in active distribution networks," *Appl. Energy*, vol. 241, pp. 613–624, 2019.

LORRANA F. DA ROCHA received the B.Sc. degree in automation and control engineering from the Federal Center for Technological Education of Minas Gerais, Brazil, in 2018. She received the M.Sc. degree in electrical engineering from the Federal University of Juiz de Fora, Brazil, in 2020. She is currently working toward the Ph.D. degree with the Norwegian University of Science and Technology working on design of power electronics architecture and control methods for a high-voltage direct current power train for offshore wind.

She also has a background in coordinated control of offshore systems and integration of offshore wind energy. Her research interests include power electronic converters, modeling and control strategies, and power train drive systems. In addition to the issues of lowering prices and boosting efficiency of offshore wind farms.

DANILO I. BRANDAO (Senior Member, IEEE) received the Ph.D. degree in electrical engineering from the University of Campinas, Campinas, Brazil, in 2015.

He was a Visiting Scholar with the Colorado School of Mines, USA, in 2009 and 2013, a Visiting Scholar with the University of Padova, Italy, in 2014, and a Guest Professor with the Norwegian University of Science and Technology, Norway, in 2018 and 2020. He is currently an Assistant Professor at the Graduate Program in Electrical Engineering, the Federal University of Minas Gerais, Belo Horizonte, Brazil. His main research interests are control of grid-tied converters and microgrids. He is a member of SOBRAEP.

KASSIANE DE S. MEDEIROS received the M.S. degree in electrical engineering from the Pontifical Catholic University of Minas Gerais, Belo Horizonte, Brazil, in 2015. She is currently working toward the Ph.D. degree in electrical engineering with the Federal University of Minas Gerais, Belo Horizonte, Brazil.

Her current research and technical interests include offshore energy, and power-quality issues.

MATHEUS S. DALL'ASTA was born in Curitibanos, Santa Catarina, Brazil, in 1993. He received the B.Sc. and M.Sc. degrees in electrical engineering from the Federal University of Santa Catarina, Florianópolis, Brazil, in 2017 and 2019, respectively. He is currently working toward the Ph.D. degree in electrical engineering at UFSC, in the power electronics and electrical drives area.

His research interests include microgrids, wind energy conversion systems, grid-connected inverters, and switched-capacitor converters.

TELLES B. LAZZARIN (Senior Member, IEEE) was born in Criciúma, Santa Catarina State, Brazil, in 1979. He received the B.Sc., M.Sc., and Ph.D. degrees in electrical engineering from the Federal University of Santa Catarina, Florianópolis, Brazil, in 2004, 2006, and 2010, respectively.

He is currently an Adjunct Professor with the Department of Electronic and Electrical Engineering, UFSC. In 2006, he worked with industry, including R&D activities at the WEG motor drives & controls, Brazil. He was a Postdoctoral Fellow with the UFSC, Florianopolis, Brazil, in 2011 and a Visiting Researcher with the Northeastern University, Boston, USA, from 20017 to 2018.

Dr. Lazzarin is a member of Brazilian Power Electronics Association, Power Electronics Society, Industry Applications Society, and Industrial Electronics Society. He has been an Associate Editor for the Brazilian Power Electronics Journal and IEEE Open Journal of Power Electronics since 2020.